

A constitutive model for viscosity of dense fiber suspension.A. Monsurul Khan,¹ B. Rishabh V. More,² and Arezoo M. Ardekani³¹*Department of Mechanical Engineering, Purdue University, IN 47905,**USA*²*Department of Mechanical Engineering, Massachusetts Institute of Technology,**MA 02139, USA*³*Department of Mechanical Engineering, Purdue University, IN 47905,**USA*

(*Electronic mail: ardekani@purdue.edu.)

(Dated: 15 November 2022)

We propose a constitutive model to predict the viscosity of fiber suspensions, which undergoes shear thinning, at various volume fractions, aspect ratios, and shear stresses/rates. We calibrate the model using the data from direct numerical simulation and prove the accuracy by predicting experimental measurements from the literature. We use a friction coefficient decreasing with the normal load between the fibers to quantitatively reproduce the experimentally observed shear thinning in fiber suspensions. In this model, the effective normal contact force, which is directly proportional to the bulk shear stress, determines the effective friction coefficient. A rise in the shear stress reduces the effective friction coefficient in the suspension. As a result, the jamming volume fraction increases with the shear stress, resulting in a shear thinning in the suspension viscosity. Moreover, we extend the model to quantify the effects of fiber volume fraction and aspect ratio in the suspension. We calibrate this model using the data from numerical simulations for the rate-controlled shear flow. Once calibrated, we show that the model can be used to predict the relative viscosity for different volume fractions, shear stresses, and aspect ratios. The model predictions are in excellent agreement with the available experimental measurements from the literature. The findings of this study can potentially be used to tune the fiber size and volume fraction for designing the suspension rheology in various applications.

I. INTRODUCTION:

Suspensions of fibers are found in a wide variety of applications, including mixing of elongated particles with concrete to enhance strength, tailoring the rheological properties of drilling fluids, and the production of paper from wood (Bivins *et al.*, 2005; Lundell, Söderberg, and Alfredsson, 2011; Hassanpour, Shafigh, and Mahmud, 2012; Elgaddafi *et al.*, 2012). During processing and transport, these materials are subjected to shear deformations, which cause translation, rotation, bending, and breaking of the fibers. These phenomena modify the microstructure in the suspension, which in turn affects the final product's physical and mechanical properties. Therefore, it is desirable to have an accurate prediction of the rheological characteristics of suspensions in order to optimize these processes in industrial facilities. However, rigid fiber suspensions exhibit a complex rheological behavior due to the gamut of determining variables involved, including fiber-fiber, fiber-wall, and fiber-matrix interactions, as well as events such as fiber breakage and migration. The complex rheological behavior includes non-Newtonian flow properties such as shear thinning, finite normal stress differences, yielding, and jamming (Goto, Nagazono, and Kato, 1986; Kitano and Kataoka, 1981; Bounoua *et al.*, 2016a; Snook *et al.*, 2014; Keshtkar, Heuzey, and Carreau, 2009; Tapia *et al.*, 2017), making their flow challenging to predict and control.

One of the crucial variables governing suspension rheology is fiber orientation. Hence, most of the constitutive modeling efforts to date have focused on explaining the suspension viscosity by linking fiber orientations to the suspension viscosity. Experimental measurements and theoretical analyses have shown that a higher fiber alignment with the flow results in a lower viscosity when compared to random orientation states. A close approximation of the motion of the fiber is frequently achieved by applying Jeffery's exact solution to the motion of an isolated ellipsoid in an infinite Newtonian fluid (Jeffery, 1922). Folgar and Tucker III (1984) developed the widely used variation of Jeffery's equations based on rotational diffusion and allowed for the influence of interactions on orientation. These tests from Folgar and Tucker III (1984), Stover (Stover, Koch, and Cohen, 1992), and Petrich (Petrich, Koch, and Cohen, 2000) conducted on the distribution of fiber orientation demonstrated that an increase in the fiber concentration caused a modest change in the orientation of the fibers during steady shear towards the flow-velocity-gradient plane, which led to an increase in the suspension's viscosity as a whole. Originated by Hinch and Leal (1975, 1976), the constitutive equation of fiber

orientation-induced extra stress in a Newtonian viscous matrix was developed by Dinh and Armstrong (Dinh, 1981; Dinh and Armstrong, 1984). Furthermore, Dinh-Armstrong's constitutive model has been used to predict the transient shear viscosity (Sepehr *et al.*, 2004; Eberle *et al.*, 2009); the change of fiber orientation was determined with a strain reduction factor of slowing down the orientation response (Folgar and Tucker III, 1984; Advani and Tucker III, 1990; Wang, O'Gara, and Tucker III, 2008). Moreover, Dinh-Armstrong's model has been extended in nonlinear Newtonian viscous liquids, including the Carreau model (Férec *et al.*, 2009), the power law model (Férec *et al.*, 2016), and the Bingham model (Férec *et al.*, 2017). The majority of the previous studies have focused on the dilute and semi-dilute regime; however, concentrated fiber suspensions have not been studied as much (Batchelor, 1971; Goddard, 1976a,b; Shaqfeh and Fredrickson, 1990). In concentrated suspension, direct interactions between fibers are typical. So, the constitutive model constructed for dilute/semi-dilute suspension must be modified, or new models must be reconstructed (Babkin, 1989) for the concentrated suspensions. Pipes and coworkers constructed the non-Newtonian constitutive relationships for hyper-concentrated fiber suspensions with an oriented fiber assembly. However, their model is only limited to concentrated suspensions with fibers of very large aspect ratio (>100), where the fibers are required to be arranged with a very high degree of collimation (Pipes *et al.*, 1991; Pipes, 1992; Pipes *et al.*, 1994). Moreover, the studies that only consider hydrodynamic interactions or pure mechanical contacts (Sundararajakumar and Koch, 1997) cannot predict shear-thinning rheology, hinting at the need for a complete physical understanding of micro-mechanics of fiber suspensions.

Inter-fiber interactions between nearby fibers play a significant role in determining the stress in dense fiber suspensions (Sundararajakumar and Koch, 1997; Lindström and Uesaka, 2007; Khan *et al.*, 2021). This is due to the fact that contacts produce friction and resistance to rolling motion in addition to generating normal forces between the fibers. As the contribution of frictional contacts to the suspension stress becomes dominant in concentrated suspensions, it is crucial to utilize an accurate contact model that can capture their rate-dependent rheological behavior. However, the simplified model of a constant friction coefficient employed in earlier studies may not be applicable to real fibers and hence, cannot accurately predict the rate-dependence of suspension rheology (Salahuddin, Wu, and Aidun, 2013; Lindström and Uesaka, 2008). Experimental measurements reveal that the coefficient of friction is not a constant and depends on the normal force (Brizmer, Kligerman, and Etsion, 2007; Lobry *et al.*, 2019; Khan *et al.*, 2021). Using the load-dependent friction coefficient model, it has been shown that we can quantitatively predict the

shear thinning rheology (Khan *et al.*, 2021).

In many industrial applications, carrying suspensions at high solid volume fractions is essential to maximize transportation and reduce energy consumption. Prior rheological research mainly dealt with suspensions at relatively small volume fractions (Folgar and Tucker III, 1984; Advani and Tucker III, 1990; Petrie, 1999; Bibbó, 1987; Chaouche and Koch, 2001; Salahuddin, Wu, and Aidun, 2013). The prediction of Phan *et al.* (Phan-Thien, Zheng, and Graham, 1991) agrees reasonably well with the Miliken *et al.* (Forth, 1989) data of relative viscosity at a volume fraction less than 10%. At moderately higher volume fractions, it was observed that the specific viscosity increased with the cube of the volume fraction. The constitutive model for dilute suspensions (Giesekus, 1962; Leal and Hinch, 1971; Hinch and Leal, 1973) can only predict that the specific viscosity is proportional to the volume fraction; the transition from linear to cubic behavior in the relative viscosity vs. the volume fraction is beyond the scope of the dilute-suspension theory. Consequently, this constitutive model for dilute suspensions was extended to the semi-dilute regime to capture the suspension's transition from linear to cubic behavior (Phan-Thien and Graham, 1991). However, to the best of the author's knowledge, there has been no constitutive model to capture the relative viscosity of the concentrated suspensions. Furthermore, for fibers with large aspect ratios ($AR = L/d$, where L and d are the fiber length and diameter, respectively), it is challenging to identify rheology measurements for volume fractions above 0.10. Measurements are only available for volume fractions up to $\phi = 0.15$ or $\phi = 0.17$ (Bibbó, 1987; Bounoua *et al.*, 2016b), even for aspect ratios as high as 17 or 18, while Bibbó *et al.* (Bibbó, 1987) made measurements as high as $\phi = 0.23$ for smaller aspect ratios of $AR = 9$. Additionally, the volume fraction for non-colloidal fibers at which the shear stresses diverge, and the flow of the suspension ceases (i.e., jams) was only determined for a lower aspect ratio, $AR = 14$ (Tapia *et al.*, 2017). Therefore, it is challenging to describe and predict the rheological characteristics of suspensions close to jamming at different aspect ratios due to the lack of a model accurately capturing the underlying physics.

This paper aims to resolve these limitations by quantifying the effect of increasing volume fraction, coefficient of friction, and fiber aspect ratio on the rheology of relatively rigid fiber suspensions using constitutive equations that can accurately capture these effects. We perform extensive numerical simulations by varying the volume fraction, aspect ratio, coefficient of friction, and shear rate. Informed by the numerical results, we propose a viscosity model that expresses the suspension rheology in terms of the shear stress and the fiber aspect ratio. The proposed model is based on two diverging stress-independent rheological behaviors, where a function of stress

can interpolate the properties between two extremes. To this end, we briefly discuss the governing equations, inter-fiber interactions, and simulation conditions in Sec. II. We then illustrate the constitutive model in Sec. III. Finally, in Sec. IV, we demonstrate the efficacy of the model by applying it to our simulation data in predicting the suspension rheology. The model requires the knowledge of rheological data at low and high shear limits along with an interpolating function of applied shear stress to predict the relative viscosity at intermediate stress values.

II. METHODOLOGY:

This section describes the models and algorithms used to simulate the shear flow of the suspension of fibers. We consider a suspension of N fibers of aspect ratio AR in a shear flow with top and bottom walls moving in the opposite direction with imposing a shear rate $\dot{\gamma}$. We have used the same numerical method to simulate the dense fiber suspensions as in our previous study (Khan *et al.*, 2021).

A. Governing equations

As the fibers are suspended in a fluid flow, the hydrodynamic forces acting on the fibers need to be related to their deformation to get their configuration in the flow. Thus, the elasticity equation of slender bodies is solved. Next, the governing equations for fluid flow and motion of flexible fibers are introduced.

1. Fluid flow

The suspending fluid is considered an incompressible viscous fluid with a constant density that is governed by the Navier-stokes equations and the continuity equation.

$$\frac{\partial \mathbf{u}}{\partial t} + \nabla \cdot (\mathbf{u} \otimes \mathbf{u}) = -\nabla p + \frac{1}{Re} \nabla^2 \mathbf{u} + \mathbf{f}, \quad (1)$$

$$\nabla \cdot \mathbf{u} = 0, \quad (2)$$

where \mathbf{u} is the velocity field, p is the pressure, \mathbf{f} is the volume force arises from the interactions of the suspending fibers, and $Re = \rho \dot{\gamma} L^2 / \eta$ is the Reynolds number, where ρ is the density of the fluid, η is the dynamic viscosity of the suspending fluid, and L is the characteristic length scale which is also the fiber length.

2. Dynamics of flexible slender bodies

As the fibers are considered continuous one-dimensional objects, Euler-Bernoulli equations can be derived for the motion of flexible fibers as (Segel and Handelman, 2007) :

$$\Delta\rho \frac{\partial^2 \mathbf{X}}{\partial t^2} = \frac{\partial}{\partial s} \left(T \frac{\partial \mathbf{X}}{\partial s} \right) - \frac{\partial^2}{\partial s^2} \left(B^* \frac{\partial^2 \mathbf{X}}{\partial s^2} \right) + \Delta\rho \mathbf{g} - \mathbf{F} + \mathbf{F}^f, \quad (3)$$

where s is the curvilinear coordinate along the fiber, \mathbf{X} is the position of the Lagrangian points on the fiber axis, T the tension, $B^* = EI$ the bending rigidity with E the modulus of elasticity of the fiber and I the second moment of inertia around the filament axis, \mathbf{g} is the gravitational acceleration, \mathbf{F} is the fluid-solid interaction force per unit length on the fiber by the surrounding fluid, and \mathbf{F}^f is the net interaction force on the fiber due to neighboring fibers. Finally, $\Delta\rho$ is the linear density difference between the fiber and the surrounding fluid defined as:

$$\Delta\rho = \rho_f - \rho A_f, \quad (4)$$

where ρ_f is the actual fiber linear density, and A_f is the sectional area of the fiber. The fibers are considered as inextensible but can bend (Huang, Shin, and Sung, 2007; Pinelli *et al.*, 2017). The inextensible constraint is expressed as :

$$\frac{\partial \mathbf{X}}{\partial s} \cdot \frac{\partial \mathbf{X}}{\partial s} = 1. \quad (5)$$

For the case of neutrally buoyant fiber, $\Delta\rho = 0$. Therefore, the left-hand side and the gravitational term on the right-hand side go to zero. For a neutrally buoyant case, the non-dimensional form of Eq. 5 remains unchanged and Eq. 3 can be expressed as :

$$0 = \frac{\partial}{\partial s} \left(T \frac{\partial \mathbf{X}}{\partial s} \right) - \frac{\partial^2}{\partial s^2} \left(B \frac{\partial^2 \mathbf{X}}{\partial s^2} \right) - \mathbf{F} + \mathbf{F}^f \quad (6)$$

with the following characteristics scales: L for length, $U_\infty = \dot{\gamma}L$ for velocity, $\dot{\gamma}^{-1}$ for time, ρ_f for reference density, $\rho_f L^2 \dot{\gamma}^2$ for tension, and $\rho_f \dot{\gamma}^2 L$ for force. Therefore, the dimensionless bending stiffness $B = \frac{B^*}{\rho_f \dot{\gamma}^2 L^4}$ measures the ratio of the convective time scale to the elastic time scale. So, as B decreases, fibers become more flexible. In this study, we fix B at a higher value which ensures a negligible bending of the fiber. Since the left-hand side of Eq. 6 is zero, in order to avoid singularity in the coefficient matrix, the equation is modified as:

$$\frac{\partial^2 \mathbf{X}}{\partial t^2} = \frac{\partial^2 \mathbf{X}_{fluid}}{\partial t^2} + \frac{\partial}{\partial s} \left(T \frac{\partial \mathbf{X}}{\partial s} \right) - B \frac{\partial^4 \mathbf{X}}{\partial s^4} - \mathbf{F} + \mathbf{F}^f, \quad (7)$$

where the first term on the right-hand side is the fluid particle acceleration which is identical to the left-hand side for the neutrally buoyant fibers. As the fibers are suspended in the fluid medium, we impose zero force, moment, and tension at the free ends.

$$\frac{\partial^2 \mathbf{X}}{\partial s^2} = 0, \frac{\partial^3 \mathbf{X}}{\partial s^3} = 0, T = 0 \quad (8)$$

Finally, We use the immersed boundary method (IBM) (Peskin, 1972) to couple the fluid and solid fibers' motions. For the details of the numerical method, the readers are referred to our previous publication (Khan *et al.*, 2021).

B. Short range interactions:

Even though the hydrodynamic interactions are well resolved using the IBM, the short-range interactions need a fine Eulerian mesh that increases computational cost. So, we use the proposed model to calculate the short-range interactions. The short-range interaction, $\mathbf{F}^f = \mathbf{F}^{lc} + \mathbf{F}^c$, is split into lubrication correction \mathbf{F}^{lc} and contact force \mathbf{F}^c , respectively. The implementation of lubrication correction \mathbf{F}^{lc} can be found in our previous study (Khan *et al.*, 2021).

1. Contact force

With increasing volume fraction, the surrounding fibers hinder the free rotation of fibers, giving rise to fiber-fiber contacts that influence the microstructure. Microstructure influences the macroscopic rheological properties of the suspension, such as relative viscosity. We model the contact interaction between the fibers as it is done in the discrete element method (DEM). We assume that the contact between the fibers takes place through hemispherical asperity. The asperity deformation is defined by surface overlap $\delta = h - h_r$, and contact happens when $\delta \leq 0$. Here, h is the inter-fiber surface separation, and h_r is the surface roughness, as shown in figure 1. The deformation of asperities results in normal, \mathbf{F}_n , and tangential, \mathbf{F}_t force on the fiber surface. The normal contact force \mathbf{F}_n is given by the Hertz law:

$$\mathbf{F}_n = -F_0 \left(\frac{|\delta|}{L} \right)^{3/2} \mathbf{n}, \quad (9)$$

where $F_0/L^{3/2}$ is the normal stiffness that can be evaluated as a function of fiber's mechanical properties such as elastic modulus, Poisson's ratio, Young's modulus, and roughness size (Lobry *et al.*,

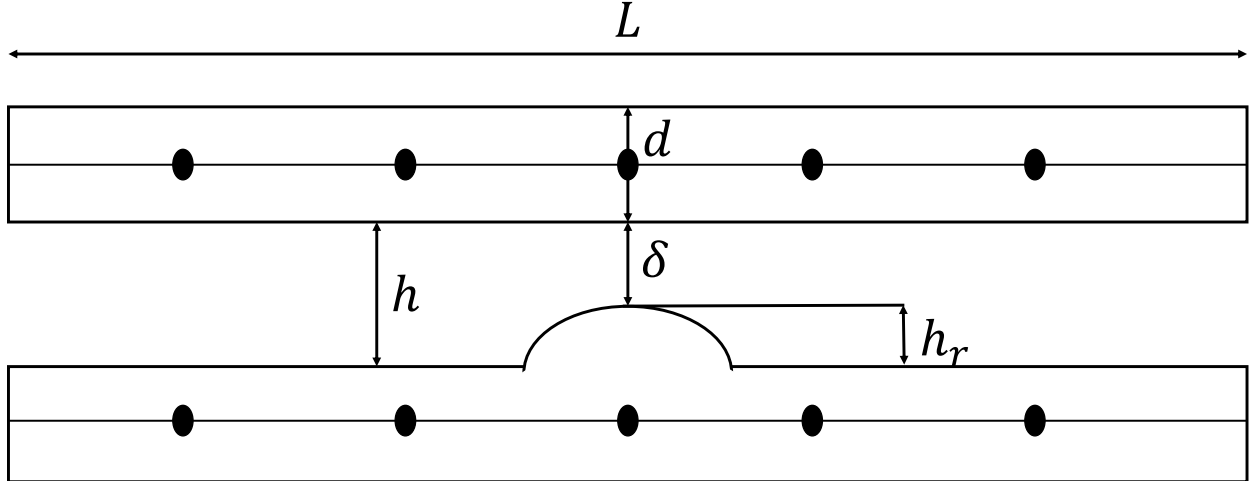


FIG. 1: A sketch of the roughness model, L and d are the length and diameter of the fiber, respectively, h_r is the roughness height, and $\delta = h - h_r$ is the surface overlap. Contact occurs when $\delta \leq 0$. Dots along the axes of the fibers indicate Lagrangian points.

2019; More and Ardekani, 2020b). In this study, we use F_0 as the characteristic contact force scale. Coulomb's friction law gives the tangential force:

$$\mathbf{F}_t = \mu |\mathbf{F}_n| \frac{\mathbf{F}_t}{|\mathbf{F}_t|}, \quad (10)$$

where μ is the friction coefficient.

2. Friction model

Researchers have utilized a constant friction coefficient when examining the dynamics of fiber suspensions numerically (Stickel *et al.*, 2009; Banaei, Rosti, and Brandt, 2020). However, a constant coefficient fails to predict the shear rate-dependent suspension viscosity. In practice, the coefficient of friction depends on many factors, such as the fiber material and the roughness size, which are implicitly included in the normal force via the normal stiffness $F_0/L^{3/2}$ (Lobry *et al.*, 2019; More and Ardekani, 2020b). Hence, a normal load-dependent coefficient of friction is a more accurate physical description of μ than a simple constant. We use the Brizmer model (Brizmer, Kligerman, and Etsion, 2007) for μ , derived from the measurements between a hemisphere and a flat surface and validated using the finite element analysis (Brizmer, Kligerman, and Etsion, 2007), which makes it applicable to a wide range of materials and conditions (Brizmer, Kligerman, and Etsion, 2007; Lobry *et al.*, 2019; More and Ardekani,

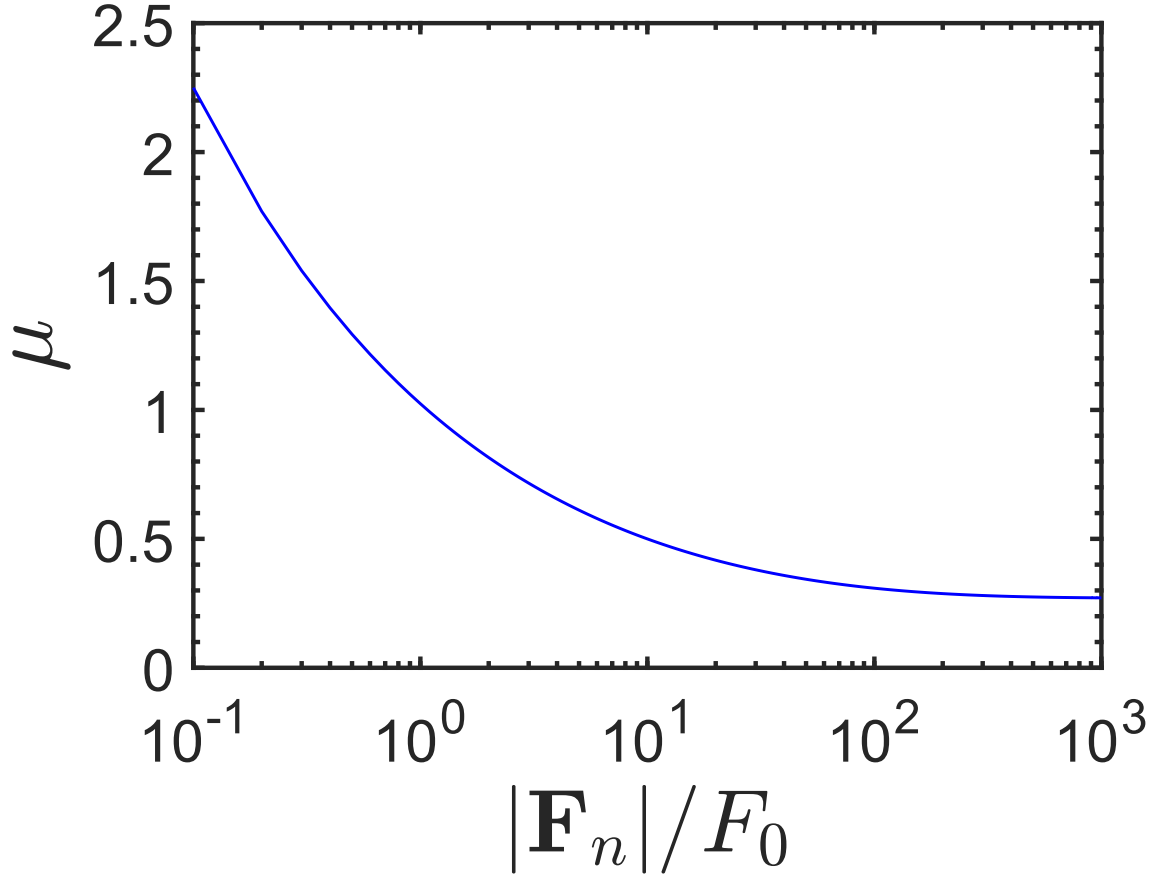


FIG. 2: Friction coefficient μ as a function of the dimensionless contact normal force (Eq. 11).

2020b). It is given by:

$$\mu = 0.27 \coth \left[0.27 \left(\frac{|\mathbf{F}_n^{(i,j)}|}{F_0} \right)^{0.35} \right], \quad (11)$$

where F_0 is the characteristic contact force scale introduced in Eq. 9. Eq. 11 is a decreasing function of $|\mathbf{F}_n^{(i,j)}|/F_0$ as illustrated in figure 2. Thus, the coefficient of friction decreases with increasing the normal force (which is equivalent to increasing asperity deformation from Eq. 9) between the contacting fibers and attains a plateau at high normal load values. Before we address the fibers with load-dependent friction coefficient, we will present results with constant μ . This will help to quantitatively understand the original case of load-dependent friction.

C. Stress and bulk rheology calculation

We compute the bulk stress in the suspension by volume averaging the viscous fluid stress and the stress generated by the presence of fibers and inter-fiber interactions. The calculation of bulk stress, including different contributions, is described elsewhere (Banaei, Rosti, and Brandt, 2020; Khan *et al.*, 2021). In this work, we present the relative viscosity to define the rheological behavior of the suspension. The relative viscosity η_r is defined as:

$$\eta_r = \frac{\eta_{eff}}{\eta}, \quad (12)$$

where η_{eff} is the effective viscosity of the suspension. The relative viscosity in terms of bulk stress is:

$$\eta_r = 1 + \Sigma_{xy}^f, \quad (13)$$

where Σ_{xy}^f is time and space averaged shear stress arising from the presence of the fibers. Σ_{xy}^f is non-dimensionalized by the product of suspending fluid viscosity η and shear rate $\dot{\gamma}$. As F_0 is considered as the characteristic contact force scale, the shear rate scale is given by $\dot{\gamma}_0 = F_0/\pi\eta d^2$. The dimensionless shear rate provides an estimate of the relative importance of contact to the hydrodynamic forces defined as:

$$\dot{\Gamma} = \frac{\dot{\gamma}}{\dot{\gamma}_0} = \frac{\dot{\gamma}}{F_0/\pi\eta d^2}, \quad (14)$$

Being the characteristic stress scale $\sigma_0 = F_0/\pi d^2$, the dimensionless stress can be defined as:

$$\tilde{\sigma} = \frac{\sigma}{\sigma_0} = \frac{\dot{\gamma}}{\dot{\gamma}_0} \Sigma_{xy} = \dot{\Gamma} \eta_r, \quad (15)$$

D. Simulation conditions

1. Boundary conditions and domain size

The fibers are suspended in a channel with upper and lower walls moving in the opposite direction with a magnitude of $U_\infty = \dot{\gamma}L$ in the x-direction. The wall is subjected to no-slip and no-penetration boundary conditions, and periodicity is assumed in the stream-wise (x) and span-wise (z) directions. Initially, we place fibers randomly in the simulation domain of size $5L \times 5L \times 8L$ and $80 \times 80 \times 128$ grid points in the stream-wise (x), wall normal (y), and span-wise direction (z), respectively. A schematic diagram of the computational configuration and coordinate system is shown in figure 3. The averaged steady state suspension viscosity changes minimal (less than 2

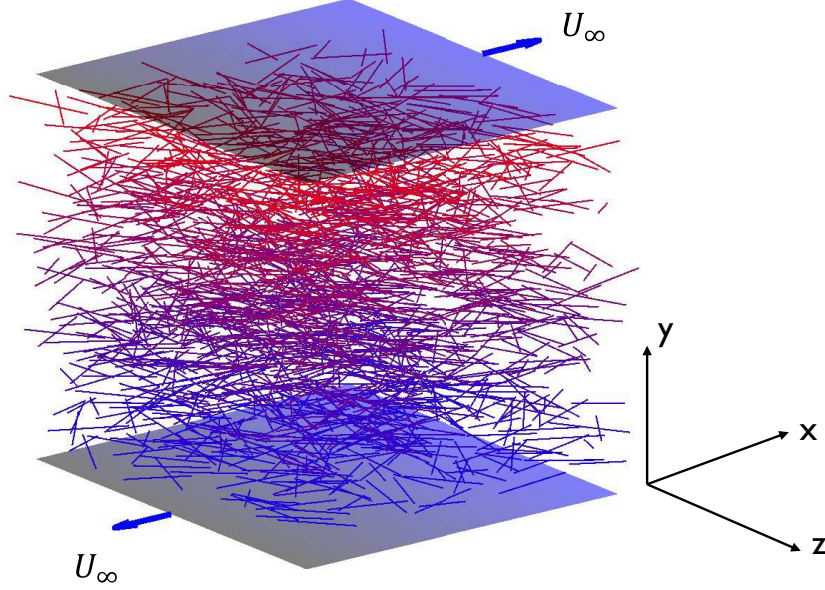


FIG. 3: Simulation setup of the shear flow of a fiber suspension. The top and bottom walls move with velocities $U_\infty = \dot{\gamma}L$ in the directions shown by the arrows.

%) in simulations with bigger domain, higher grid, and time resolutions such as 1.5, 2, 2.5, and 3 times the current domain, grid, and time resolution, Moreover, 36 Lagrangian points over the fiber length are enough to resolve the case with the highest fiber aspect ratio. The required time step to capture the fiber dynamics is $\Delta t = 10^{-5}$. The suspension is simulated until a statistically steady viscosity is observed and mean values after discarding the initial transients are presented.

2. Range of parameters investigated

The aim of this study is to quantify the effect of varying fiber aspect ratios, volume fractions, and shear rates on the rheology of the suspension. Hence, we simulate suspensions of almost rigid fibers in a shear flow by varying the aspect ratio in the range of $10 \leq AR \leq 36$. The simulations were carried out for dimensionless shear rate in the range of $0.1 \leq \dot{\gamma}/\dot{\gamma}_0 \leq 100$ for a range of volume fractions $0.03 \leq \phi \leq 0.45$. The dimensionless bending rigidity, B , was set to 5.0 which

TABLE I: Range of parameters explored in this study

ϕ	AR	$\dot{\gamma}/\dot{\gamma}_0$	μ
0.03 – 0.47	10 – 36	0.1 – 100	0 – 11

ensures a negligible bending of the fiber. The range of parameters explored in the present work is summarized in table I.

III. THE CONSTITUTIVE MODEL:

We first demonstrate simulations where the friction coefficient is maintained constant before addressing the fibers with a load-dependent friction coefficient. Thus, we reflect on the significant impact of this microscopic parameter on the suspension viscosity. Recent numerical investigations on frictional non-Brownian particle suspensions have shown that the friction coefficient, considered constant, has a significant impact on the effective viscosity (Mari *et al.*, 2014; Gallier *et al.*, 2014; Gallier, Peters, and Lobry, 2018; Singh *et al.*, 2018). From these studies, it is clear that the jamming volume fraction depends significantly on the friction coefficient. More recently, Singh *et al.* (2018) explained how the viscosity of non-colloidal suspensions changes with the microscopic particle friction coefficient by showing that the jamming volume fraction decreases when the microscopic particle friction coefficient goes from 0 to 1. We point out that simulations of granular flows (Silbert, 2010) and experiments with discontinuous shear-thickening suspensions (Fernandez *et al.*, 2013) have shown that there is a link between the amount of jamming and the microscopic friction coefficient. Therefore, we start our analysis by deriving correlation laws for the dependence of suspension jamming fraction with constant friction coefficients. After that, the correlation laws will be utilized to describe the rheology of suspensions for cases with load-dependent friction.

In the beginning, we report the simulations for suspensions of fibers in which the friction coefficient is held at a fixed value in the range of 0 to 15. The following correlation law is fitted for each value of μ to describe the variation of the relative viscosity against the volume fraction.

$$\eta_r(\mu, \phi, AR) = \alpha(\mu, AR) \left(1 - \frac{\phi}{\phi_m(\mu, AR)} \right)^{-0.90}, \quad (16)$$

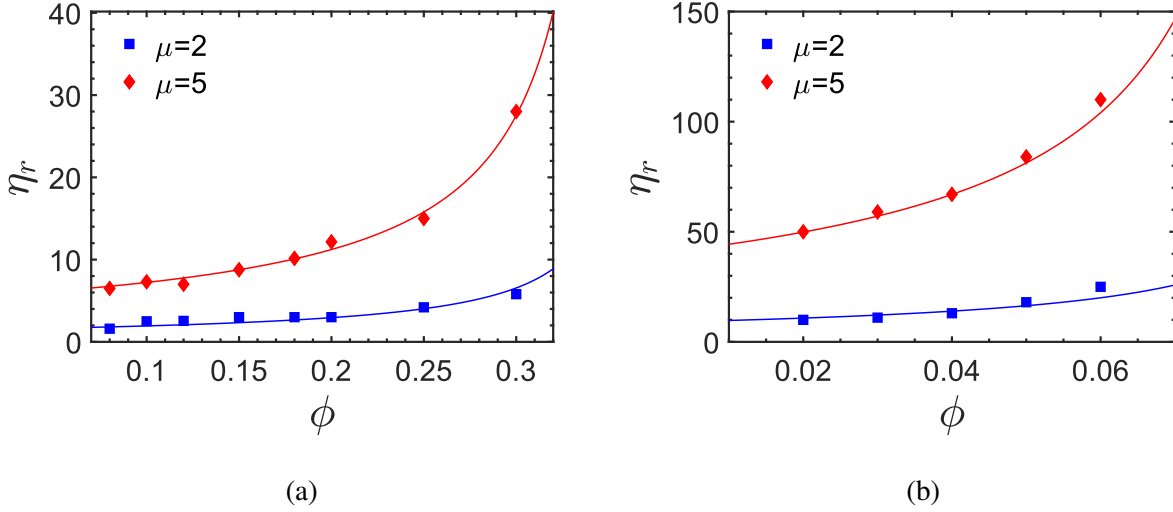


FIG. 4: Relative viscosity as a function of volume fraction for friction coefficient $\mu = 2, 5$ for (a) $AR = 10$ and (b) $AR = 36$. Solid lines: best fit with Eq. 16

where α and ϕ_m are friction and aspect ratio dependent constant coefficients. Here, we model the dependence of viscosity on volume fraction as $\phi_m^{-0.90}(\phi_m - \phi)^{-0.90}$. The form is consistent with the proposed relationships in the recent work concerning the suspension of fibers (Khan *et al.*, 2021; Tapia *et al.*, 2017). Figure 4 presents the results of the simulation along with the relevant correlation laws for two different values of the friction coefficient ($\mu = 2$ and $\mu = 5$) for aspect ratios $AR = 10$ and $AR = 36$. The friction and aspect ratio dependent parameters (α and ϕ_m) are found empirically from our simulations as:

$$\alpha(\mu, AR) = \alpha^{\mu_\infty}(AR) + \left(\alpha^{\mu_0}(AR) - \alpha^{\mu_\infty}(AR) \right) \frac{\exp(-X^\alpha \text{atan}(\mu)) - \exp(-\pi X^\alpha / 2)}{1 - \exp(-\pi X^\alpha / 2)}, \quad (17)$$

$$\phi_m(\mu, AR) = \phi_m^{\mu_\infty}(AR) + \left(\phi_m^{\mu_0}(AR) - \phi_m^{\mu_\infty}(AR) \right) \frac{\exp(-X^q \text{atan}(\mu)) - \exp(-\pi X^q / 2)}{1 - \exp(-\pi X^q / 2)} \quad (18)$$

as shown by fits in figure 5. Here, the superscript μ_0 and μ_∞ denote the corresponding parameter when the coefficient of friction is zero and infinity (Lobry *et al.*, 2019). Note that all the parameters are independent of the coefficient of friction and are reported in table II. In particular, for

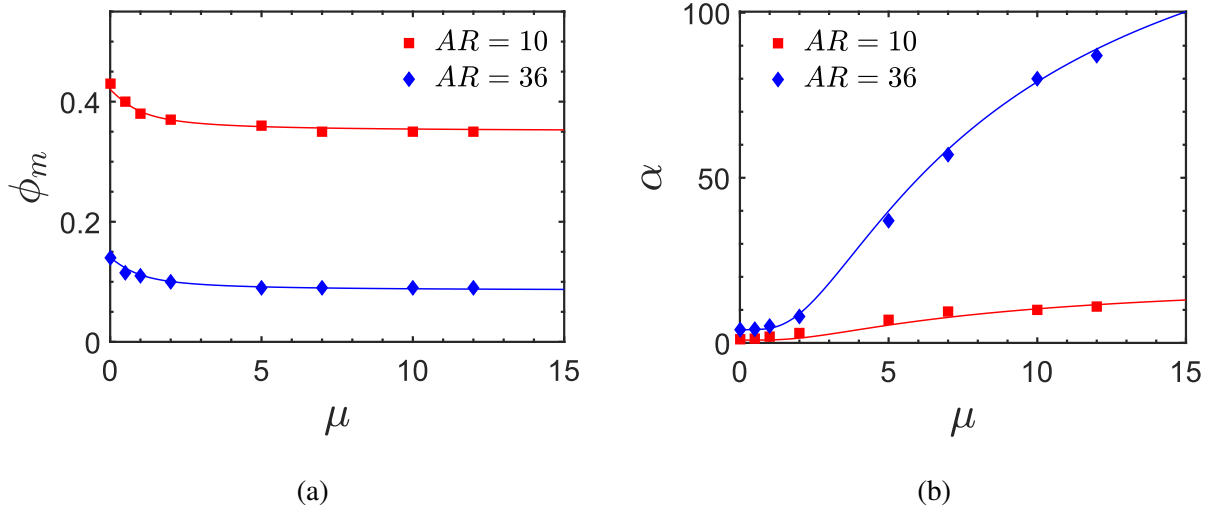


FIG. 5: (a) Jamming volume fraction ϕ_m (b) pre-factor α as a function of μ . Solid lines: best fit with Eq. 18.

TABLE II: Calibrated model parameters for Eq. 18 for aspect ratios $AR = 10$ and $AR = 36$

AR	ϕ_m^0	ϕ_m^∞	X^q	α^0	α^∞	X^α
10	0.40	0.47	0.11	0.85	20.9	-7.532
36	0.12	0.17	0.11	0.8015	0.82	-7.532

aspect ratio 18, the jamming volume fraction seems to approach the limit $\phi_m^\infty = 0.47$ as the friction coefficient goes to ∞ and is equal to $\phi_m^0 = 0.40$ for $\mu = 0$. These values are consistent with the data found in the literature (Williams and Philipse, 2003; Khan *et al.*, 2021).

The above analysis shows that the simulations with a constant friction coefficient do not provide rate-dependent viscosity in the suspension. Hence, We now turn to the analysis with load-dependent friction between the fibers in the suspension. However, the correlation derived earlier with a constant coefficient of friction will aid quantitative analysis of the case with a load-dependent friction coefficient.

From the shear rate-dependent viscosity, we observe that as the reduced shear rate increases, the viscosity decreases due to the reduction of friction coefficient (Khan *et al.*, 2021). It is possible to gain a better understanding of this transition from high to low viscosity by examining the average friction coefficient, μ_{avg} , as a function of the reduced shear stress, $\tilde{\sigma}$ ($\eta_r \dot{\gamma} / \dot{\gamma}_0$), as shown in figure 6.

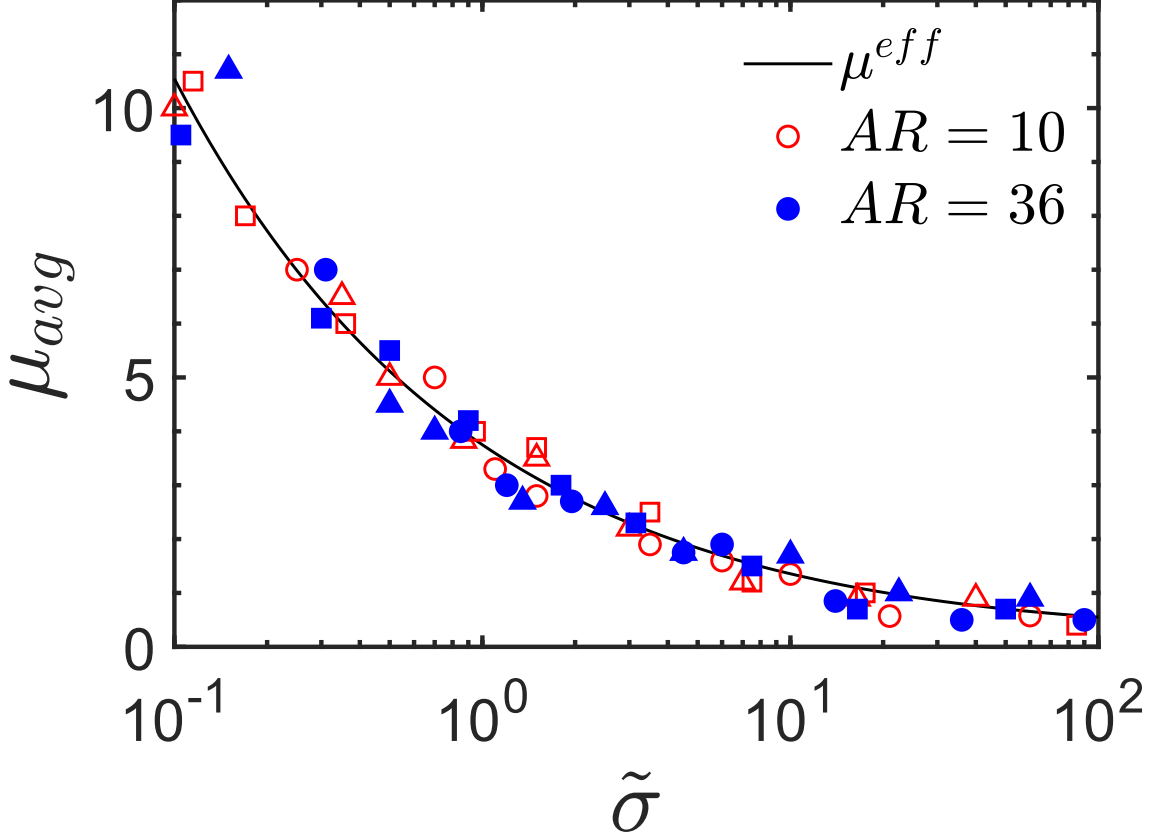


FIG. 6: Average coefficient of friction over all contacting fiber pairs as a function of shear stress.

Red symbol corresponds to data for $AR = 10$ having volume fractions (\square) $\phi = 0.20$, (\triangle) $\phi = 0.30$, and (\circ) $\phi = 0.35$. Blue symbol corresponds to data for $AR = 36$ having volume fractions (\blacksquare) $\phi = 0.03$, (\blacktriangle) $\phi = 0.05$, and (\bullet) $\phi = 0.08$. The solid line shows the effective coefficient of friction from Eq. 19.

Reduced shear stress $\tilde{\sigma}$ quantifies the typical force experienced by two contacting fibers, and μ_{avg} is the ensemble average of the coefficient of friction μ between all the contacting fiber pairs in the suspension. Intriguingly, regardless of the fiber volume fraction and aspect ratio, the data collapse onto a single curve, denoted by μ^{eff} , fitted with:

$$\mu^{eff} = 0.34 \coth \left[0.35 \left(\frac{\tilde{\sigma}}{20} \right)^{0.45} \right]. \quad (19)$$

The functional form is similar to the one for the coefficient of friction μ dependence on the normal load between the fibers $|\mathbf{F}_n^{(i,k)}|$ in Eq. 11, however, it is not exactly the same. This feature is not immediately apparent; thus, it is worth commenting on. The normal contact force does regulate

the microscopic coefficient of friction between contacting fibers. However, the bulk shear stress and mean force are only qualitatively related. Even the relationship between the mean friction coefficient and mean force is difficult to predict due to the highly non-linear relationship between the microscopic friction coefficient and force. This implies that the reduced shear stress may be interpreted as the reduced effective normal force between contacting fibers, which regulates the mean friction coefficient. Therefore, we obtain the following expression for suspension viscosity at a finite stress value in terms of the volume fraction ϕ , jamming volume fraction ϕ_m , and pre-factor α .

$$\eta_r(\tilde{\sigma}, \phi, AR) = \alpha \left(\tilde{\sigma}(\mu_{eff}), AR \right) \left(1 - \frac{\phi}{\phi_m(\tilde{\sigma}(\mu_{eff}), AR)} \right)^{-0.90} \quad (20)$$

The rheological properties in the two extreme stress conditions can be expressed in terms of volume fractions ϕ , jamming volume fractions $\phi_m^{0,\infty}$ and model parameters $\alpha^{0,\infty}$. Here the superscript 0 and ∞ denote the low and high shear limits, respectively.

$$\eta_r^0(\phi, AR) = \alpha^0(AR) \left(1 - \frac{\phi}{\phi_m^0(AR)} \right)^{-0.90}, \quad (21)$$

$$\eta_r^\infty(\phi, AR) = \alpha^\infty(AR) \left(1 - \frac{\phi}{\phi_m^\infty(AR)} \right)^{-0.90} \quad (22)$$

The jamming fraction ϕ_m and the pre-factor α at intermediate stress $\tilde{\sigma}$ can be calculated by interpolating their corresponding values in the low and high-stress limits (More and Ardekani, 2020a) as follows:

$$\phi_m(\sigma, AR) = \phi_m^0(AR)[1 - f(\tilde{\sigma})] + \phi_m^\infty[f(\tilde{\sigma})] \quad (23)$$

$$\alpha(\sigma, AR) = \alpha^\infty(AR)[f_1(\tilde{\sigma})] + \alpha^0[1 - f_1(\tilde{\sigma})], \quad (24)$$

where

$$\begin{aligned} f(\tilde{\sigma}) &= f(\tilde{\sigma}(\mu_{eff})) \\ &= \frac{\exp(-X^q \operatorname{atan}(\tilde{\sigma}(\mu_{eff}))) - \exp(-\pi X^q/2)}{1 - \exp(-\pi X^q/2)}, \end{aligned} \quad (25)$$

$$\begin{aligned} f_1(\tilde{\sigma}) &= f(\tilde{\sigma}(\mu_{eff})) \\ &= \frac{\exp(-X^\alpha \operatorname{atan}(\tilde{\sigma}(\mu_{eff}))) - \exp(-\pi X^\alpha/2)}{1 - \exp(-\pi X^\alpha/2)}. \end{aligned} \quad (26)$$

A similar interpolation function was used to interpolate α and ϕ_m when we considered results with a constant coefficient of friction. Later we find an expression to describe the reduced stress as a function of u^{eff} (Eq. 19). Thus, we use a similar interpolation function as expressed by $f(\vec{\sigma})$. In addition, the pre-factor α and jamming volume fraction ϕ_m in the low and high shear stress limits can be expressed in terms of aspect ratio, AR and model parameters $\{\bar{\phi}_m, \bar{\alpha}\}^{0,\infty}$, $\{\hat{\phi}_m, \hat{\alpha}\}^{0,\infty}$, $\{Q_{\alpha, \phi_m}\}^{0,\infty}$, $\{R_{\alpha, \phi_m}\}^{0,\infty}$, and $\{S_{\alpha, \phi_m}\}^{0,\infty}$. Here, the superscript 0 and ∞ denote the model parameters at low and high shear limits, respectively. We use $\bar{}$ and $\hat{}$ over model parameters for the fibers with aspect ratios 10 and 36 cases, respectively.

$$\alpha^{0,\infty} = \bar{\alpha}^{0,\infty} + \left[\hat{\alpha}^{0,\infty} - \bar{\alpha}^{0,\infty} \right] \log \left(\frac{Q_{\alpha}^{0,\infty}}{(AR)^{R_{\alpha}^{0,\infty}}} \right)^{S_{\alpha}^{0,\infty}} \quad (27)$$

$$\phi_m^{0,\infty} = \bar{\phi}_m^{0,\infty} + \left[\hat{\phi}_m^{0,\infty} - \bar{\phi}_m^{0,\infty} \right] \log \left(\frac{Q_{\phi_m}^{0,\infty}}{(AR)^{R_{\phi_m}^{0,\infty}}} \right)^{S_{\phi_m}^{0,\infty}} \quad (28)$$

The value of the calibrated model parameters is reported in table III.

IV. RESULT

A. Aspect ratio dependent rheology

Experiments (Keshtkar, Heuzey, and Carreau, 2009; Bounoua *et al.*, 2016a) and numerical simulations (Khan *et al.*, 2021; Tapia *et al.*, 2017) have shown that increasing aspect ratio leads to increased suspension viscosity due to a reduction of the jamming fraction. Figure 7 shows the relative viscosity as a function of fiber volume fraction for the long ($AR = 36$) and short ($AR = 10$) fibers in the low and high shear rate limits with the modified Maron-Pierce fitting curves [Eqs. 21,22]. As we present for $AR = 10$ and $AR = 36$ in the main text, we refer to the cases as "short" and "long" henceforth in the article. Here, the reduction in the jamming volume fraction, ϕ_m , with increasing aspect ratio and stress is consistent with experiments (Keshtkar, Heuzey, and Carreau, 2009; Bounoua *et al.*, 2016b,a; Tapia *et al.*, 2017). We observe that the calibrated model parameters and jamming volume fraction depend only on the fiber aspect

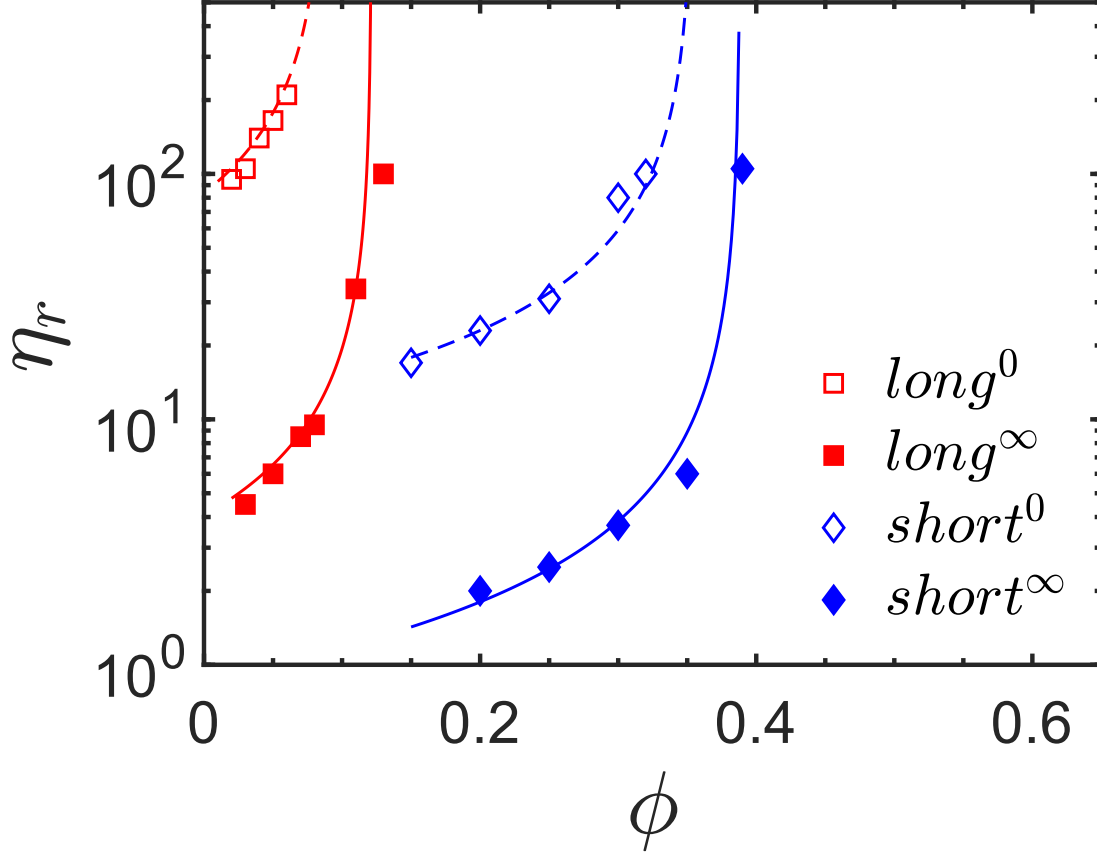


FIG. 7: Relative viscosity of the long ($AR = 36$) and short ($AR = 10$) fiber suspensions for different volume fractions. Dashed and solid lines represent fitting Eqs. in the low (0 , Eq. 21) and high ($^\infty$, Eq. 22) stress limits.

ratio in the low and high shear rate limits. So, they can be expressed in terms of AR , as shown in Eqs. (27)-(28). Figures 8a and 8b show that Eqs. (27)-(28) are a good fit and accurately capture the effect of increasing fiber aspect ratio on the rheology of the dense fiber suspensions in the low and high shear limits.

Before going into detail about stress-dependent rheology, it is important to note that aspect ratio dependence and stress dependence are unrelated. Stress-dependent rheological behavior is recovered using a load-dependent friction coefficient model, whereas aspect ratio dependence is obtained by altering the AR of the fiber. In the absence of load-dependent friction, we only get the aspect ratio dependence rheology as presented in figure 7 and modeled in Eqs. (27)-(28). We will get stress between 0 and ∞ depending on the value of μ . But the increase in viscosity with

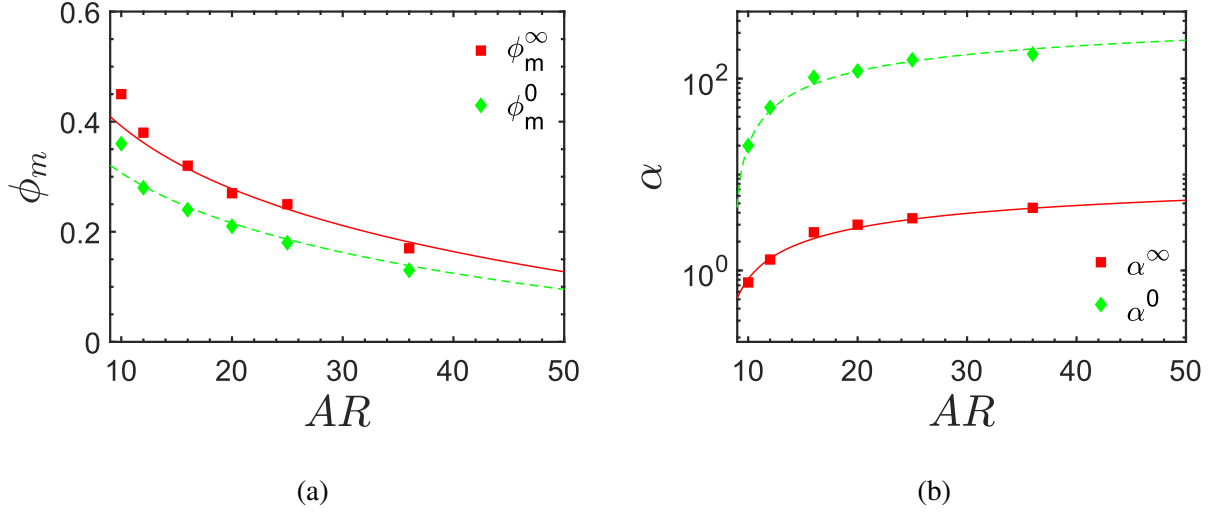


FIG. 8: Calibrated model parameters as a function of the aspect ratio of the fibers. Dashed and solid lines represent fitting Eqs. (27-28) in the low (0) and high ($^\infty$) shear limits. (a) jamming volume fraction, ϕ_m and (b) calibrated model parameter, α . An increase in the aspect ratio leads to an increase in α in both the low and high shear rate limits. However, increasing the aspect ratio reduces the jamming volume fraction, ϕ_m due to the increase in relative viscosity (Keshtkar, Heuzey, and Carreau, 2009; Tapia *et al.*, 2017; Khan *et al.*, 2021).

TABLE III: Aspect ratio dependent calibrated model parameters for relative viscosity, η_r .

	$\{\}^0$	$\{\}^0$	$Q_{\{\}}^0$	$R_{\{\}}^0$	$S_{\{\}}^0$	$\{\}^\infty$	$\{\}^\infty$	$Q_{\{\}}^\infty$	$R_{\{\}}^\infty$	$S_{\{\}}^\infty$
α	145	15	2.04	1.3	0.85	4	0.75	82.35	1.25	0.70
ϕ_m	0.23	0.70	57	1.4	0.20	0.2	0.57	82	1.27	0.35

aspect ratio will still be observed, which is consistent with earlier simulations (Wu and Aidun, 2010; Khan *et al.*, 2021) and experiments (Keshtkar, Heuzey, and Carreau, 2009; Bounoua *et al.*, 2016a; Tapia *et al.*, 2017).

B. Stress dependent viscosity

In this section, we present the shear stress-dependent viscosity for suspensions with varying fiber aspect ratios along with the constitutive equations fitting curves. It has been demonstrated

that the rheological properties in the intermediate stress values can be interpolated once the rheological characteristics and the jamming fraction in the low and high shear stress limits are known (Singh *et al.*, 2018; More and Ardekani, 2020a). Section III proposes aspect ratio and stress-dependent constitutive equations based on this premise.

Figure 9 shows the shear rate dependent relative viscosity for the short ($AR = 10$) and long ($AR = 36$) fiber suspensions for the volume fractions investigated in the study. The proposed model accurately predicts relative viscosity in the intermediate stress ($\tilde{\sigma}$) regime for both aspect ratios. It follows from this model that the reduced force that controls friction, and consequently the suspension relative viscosity, is proportional to the reduced shear stress:

$$\frac{F_n}{F_0} = \frac{\pi\eta\eta_r d^2 \dot{\gamma}}{20F_0} = \frac{\eta_r(\dot{\gamma}/\dot{\gamma}_0)}{20} = \frac{\tilde{\sigma}}{20} \quad (29)$$

We can use the values of calibrated parameters obtained from the simulation data to predict the stress-dependent relative viscosity of fiber suspensions with aspect ratio 17. The prediction is compared to the experimental data from Bibbó (1987), as shown in figure 9c. The model does a satisfactory job of capturing the relative viscosity of the experimental system. For this comparison, we assume $\sigma_0 = 0.45$ to non-dimensionalize the experimental stress. Finally, we predict the volume fraction-dependent viscosity at a high shear rate for aspect ratios 17 and 51 and compare it with Bibbó (1987), as shown in figure 9d. The data was only available in the semi-concentrated regime, and our simulation did a good job of capturing the experimental data.

Finally, due to the agreement between the results from the load-dependent friction simulations and the viscosity from Eq. 20, it is possible to estimate the effective coefficient of friction, μ_{eff} , in the experiment without running new simulations. Once we know the jamming volume fraction from the experiments, μ_{eff} can be computed by reversing Eq. 18. In this case, μ_{eff} is actually the microscopic friction coefficient for the applied load, $F_n = \pi * d^2 \sigma / 20$, where σ is the experimental stress. For the reported experiment of Bibbo *et al.* (Bibbó, 1987), we find the coefficient friction to be 1.12. We note that it is possible to deduce μ_{eff} from the viscosity measurements only if the values of the experimental jamming fraction belong to the variation range of ϕ_m , deduced from the numerical simulations at constant friction coefficient. It is important to remember that the friction coefficient values derived from the viscosity measurements are estimates.

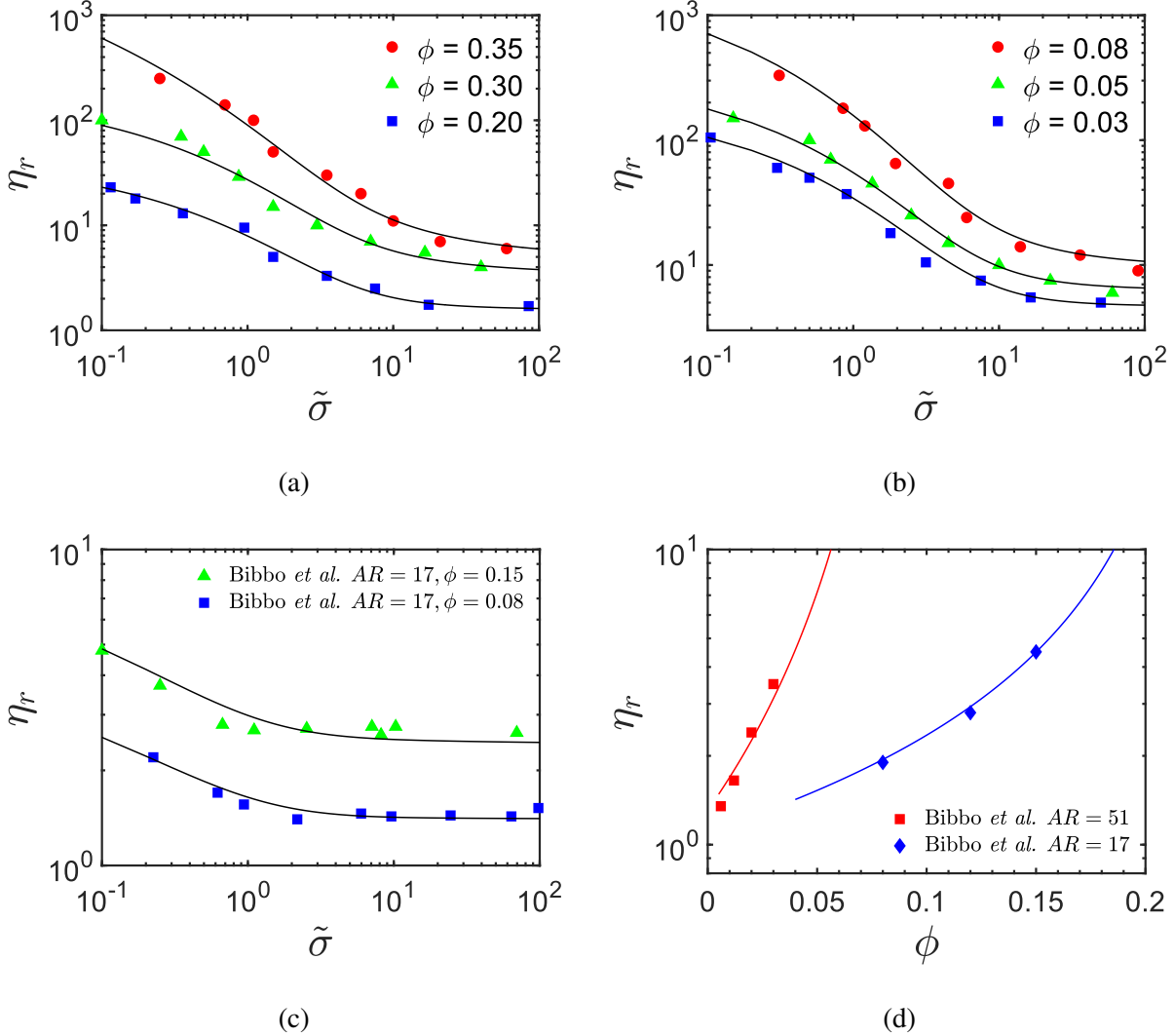


FIG. 9: Relative viscosity as a function of dimensionless shear stress, $\tilde{\sigma}$: (a) for fiber aspect ratio, $AR = 10$ and (b) for fiber aspect ratio, $AR = 36$. (c) & (d) Comparison of the constitutive model with the experimental data from Bibbo *et al.* (Bibbó, 1987). The shear stress was fixed to $\tilde{\sigma} = 0.02$ when comparing the volume fraction-dependent relative viscosity with the experimental data. The solid lines represent Eq. 20 with the values of the calibrated model parameters obtained using the simulation data.

C. Flow state diagram

The shear rheology described above is controlled by three dimensionless parameters, namely, dimensionless shear stress $\tilde{\sigma}$, volume fraction ϕ , and aspect ratio AR . The results discussed in the

paper are presented in a flow state diagram in figure 10. Here in the $\tilde{\sigma} - \phi$ phase space, we identify ϕ_m^∞ , ϕ_m^0 , and $\phi_m(\tilde{\sigma})$. In the lower part of the diagram, when the stress is too low, and in the upper part of the diagram, when the stress is large, rheology diverges at ϕ_m^0 , and ϕ_m^∞ , respectively. So in the two extremes, the relative viscosity is rate-independent. In between, we observe rate-dependent viscosity.

Moreover, the volume fraction at which the suspension jams increases with increasing stress. Previous studies on the suspension of fibers have reported that at low stress values, the suspension does not flow but can flow at higher stress values (Bibbó, 1987; Chaouche and Koch, 2001; Switzer III and Klingenberg, 2003; Keshtkar, Heuzey, and Carreau, 2009; Bounoua *et al.*, 2016b; Bounoua, Kuzhir, and Lemaire, 2016) meaning that the jamming volume fraction, ϕ_m depends on the shear stress. However, the exact dependence of the jamming fraction on the stress was largely unexplored. Our numerical simulation is superior in the sense that it quantifies the exact dependence of the jamming volume fraction on the applied stress denoted by the solid line in figure 10. In addition, the applicability of the model is further strengthened in capturing the dependence of jamming volume fraction on the stress for different aspect ratios.

V. CONCLUSION

This paper presents a constitutive model for frictional fiber suspensions in a steady shear flow. The proposed model quantifies the effects of three independent parameters - fiber volume fraction ϕ , dimensionless stress $\tilde{\sigma}$, and fiber aspect ratio AR . The model quantitatively predicts the viscosity of a range of aspect ratios and volume fractions once it is calibrated using the zero and high shear viscosities of just a few aspect ratio cases.

We start our analysis by deriving relations describing the dependence of jamming volume fraction on the friction coefficient to reflect the impact of this microscopic parameter on the suspension rheology. However, constant friction cannot explain the rate-dependent rheology in suspensions. Hence, we use the relations derived from the constant coefficient of friction for quantitatively comprehending the case with load-dependent friction coefficient. This approach assists us in defining the stress-dependent jamming fraction $\phi_m(\tilde{\sigma})$ by interpolating between two jamming fractions at the extreme limit of stresses, in the manner proposed by Wyart and Cates (Wyart and Cates, 2014) for shear thickening suspensions. The divergence of viscosity approaching the interpolated jamming volume fraction follows the form of the two limits, with the viscosity growing as

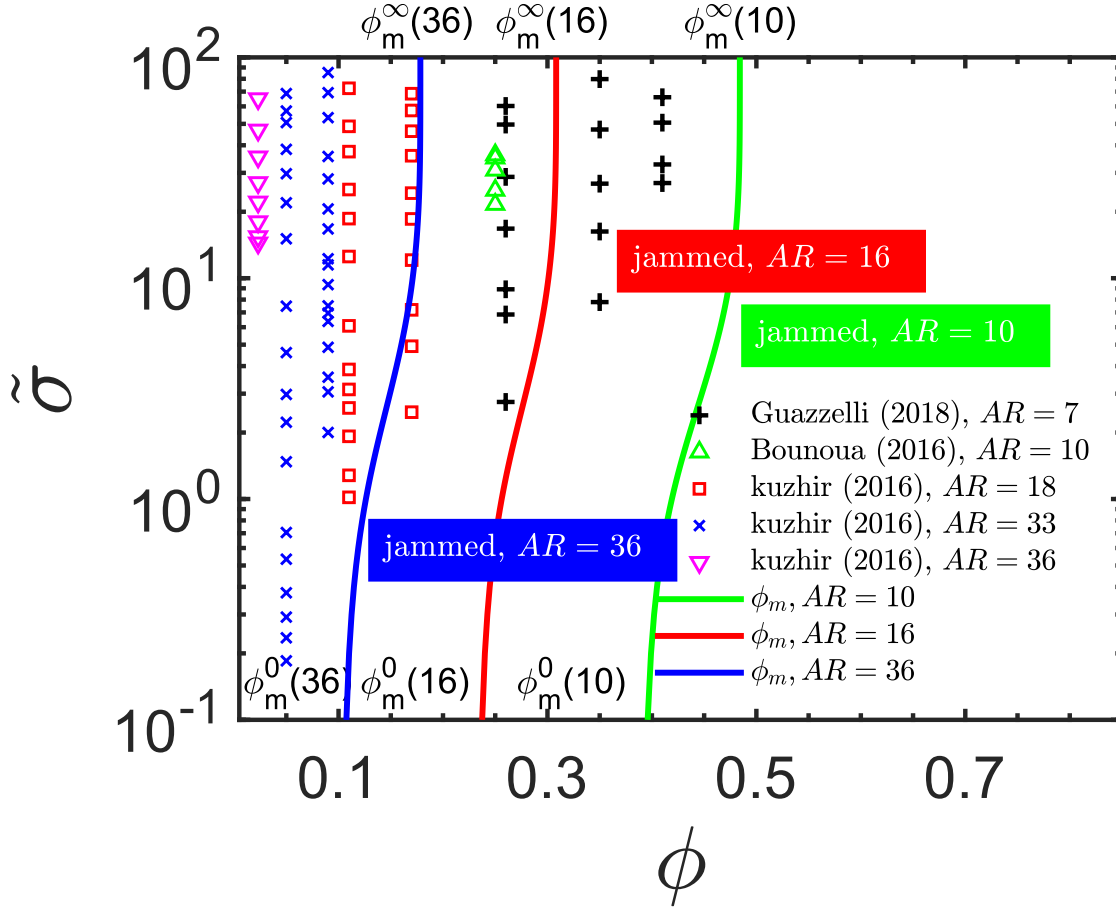


FIG. 10: $\tilde{\sigma} - \phi$ phase space diagram for fibers $AR = 10, 16,$ and 36 . Increasing aspect ratio decreases the jamming volume fraction. The suspension is jammed for the region on the right of the solid curve.

$\phi_m^{-0.90}(\phi_m - \phi)^{-0.90}$. Furthermore, we extend the constitutive model to capture the aspect ratio-dependent rheological behavior of the suspension. Once the aspect ratio-dependent rheological properties in the low and high shear limits are known, we can use the constitutive model to quantify the aspect ratio's effect on the rheology between the two stress limits. The model predictions for the relative viscosity, $\eta_r(\phi, \tilde{\sigma}, AR)$ agree well not only over the full range of parameters it is calibrated on but beyond this range as well as evident from a good agreement between experimental measurements and model predictions. In the end, we display the dependence of the jamming volume on the applied stress and aspect ratio of the fibers through a flow state diagram in the $\phi - \tilde{\sigma}$ plane.

Finally, these results can be used to quantitatively predict the shear-thinning suspension behav-

ior at different fiber aspect ratios and volume fractions. This model can be used to estimate the effective coefficient of friction in the experiment from the jamming volume fraction. The idea thus gained can be utilized in manipulating suspension behavior by changing the fiber size along with mechanisms based on hydrodynamic interactions, fiber surface roughness (Khan *et al.*, 2021), and friction (Salahuddin, Wu, and Aidun, 2013; Switzer III and Klingenberg, 2003). We found that to have higher solid concentrations desired in industrial applications, we should break down the fibers into smaller sizes or reduce the coefficient of friction through surface treatment.

ACKNOWLEDGMENTS

AMA would like to acknowledge financial support from the Department of Energy via grant EE0008910.

REFERENCES

- Advani, S. G. and Tucker III, C. L., “A numerical simulation of short fiber orientation in compression molding,” *Polymer composites* **11**, 164–173 (1990).
- Babkin, V., “Constitutive equations for a nondilute dispersed fiber suspension,” *Fluid Dynamics* **24**, 882–887 (1989).
- Banaei, A. A., Rosti, M. E., and Brandt, L., “Numerical study of filament suspensions at finite inertia,” *Journal of Fluid Mechanics* **882** (2020).
- Batchelor, G., “The stress generated in a non-dilute suspension of elongated particles by pure straining motion,” *Journal of Fluid Mechanics* **46**, 813–829 (1971).
- Bibbó, M. A., *Rheology of semiconcentrated fiber suspensions*, Ph.D. thesis, Massachusetts Institute of Technology (1987).
- Bivins, C. H., Boney, C., Fredd, C., Lassek, J., Sullivan, P., Engels, J., Fielder, E. O., Gorham, T., Judd, T., Mogollon, A. E. S., *et al.*, “New fibers for hydraulic fracturing,” *Oilfield Review* **17**, 34–43 (2005).
- Bounoua, S., Kuzhir, P., and Lemaire, E., “Normal stress differences in non-brownian fiber suspensions,” *Journal of rheology* **60**, 661–671 (2016).
- Bounoua, S., Lemaire, E., Férec, J., Ausias, G., and Kuzhir, P., “Shear-thinning in concentrated

- rigid fiber suspensions: Aggregation induced by adhesive interactions,” *Journal of Rheology* **60**, 1279–1300 (2016a).
- Bounoua, S., Lemaire, E., Férec, J., Ausias, G., Zubarev, A., and Kuzhir, P., “Apparent yield stress in rigid fibre suspensions: the role of attractive colloidal interactions,” *Journal of Fluid Mechanics* **802**, 611–633 (2016b).
- Brizmer, V., Kligerman, Y., and Etsion, I., “Elastic–plastic spherical contact under combined normal and tangential loading in full stick,” *Tribology Letters* **25**, 61–70 (2007).
- Chaouche, M. and Koch, D. L., “Rheology of non-brownian rigid fiber suspensions with adhesive contacts,” *Journal of Rheology* **45**, 369–382 (2001).
- Dinh, S. M., *On the rheology of concentrated fiber suspensions*, Ph.D. thesis, Massachusetts Institute of Technology (1981).
- Dinh, S. M. and Armstrong, R. C., “A rheological equation of state for semiconcentrated fiber suspensions,” *Journal of Rheology* **28**, 207–227 (1984).
- Eberle, A. P., Baird, D. G., Wapperom, P., and Vélez-García, G. M., “Using transient shear rheology to determine material parameters in fiber suspension theory,” *Journal of Rheology* **53**, 685–705 (2009).
- Elgaddafi, R., Ahmed, R., George, M., and Growcock, F., “Settling behavior of spherical particles in fiber-containing drilling fluids,” *Journal of Petroleum Science and Engineering* **84**, 20–28 (2012).
- Férec, J., Ausias, G., Heuzey, M., and Carreau, P., “Modeling fiber interactions in semiconcentrated fiber suspensions,” *Journal of Rheology* **53**, 49–72 (2009).
- Férec, J., Bertevas, E., Khoo, B. C., Ausias, G., and Phan-Thien, N., “The effect of shear-thinning behaviour on rod orientation in filled fluids,” *Journal of Fluid Mechanics* **798**, 350–370 (2016).
- Férec, J., Bertevas, E., Khoo, B. C., Ausias, G., and Phan-Thien, N., “A rheological constitutive model for semiconcentrated rod suspensions in bingham fluids,” *Physics of Fluids* **29**, 073103 (2017).
- Fernandez, N., Mani, R., Rinaldi, D., Kadau, D., Mosquet, M., Lombois-Burger, H., Cayer-Barrioz, J., Herrmann, H. J., Spencer, N. D., and Isa, L., “Microscopic mechanism for shear thickening of non-brownian suspensions,” *Physical review letters* **111**, 108301 (2013).
- Folgar, F. and Tucker III, C. L., “Orientation behavior of fibers in concentrated suspensions,” *Journal of reinforced plastics and composites* **3**, 98–119 (1984).
- Forth, S., “Milliken, wj, gottlieb, m., graham, al, mondy, l. a. & powell, rl the viscosity-volume

- fraction relation for suspensions of rod-like particles by falling-ball,” *Journal of Fluid Mechanics* **202** (1989).
- Gallier, S., Lemaire, E., Peters, F., and Lobry, L., “Rheology of sheared suspensions of rough frictional particles,” *Journal of Fluid Mechanics* **757**, 514–549 (2014).
- Gallier, S., Peters, F., and Lobry, L., “Simulations of sheared dense noncolloidal suspensions: Evaluation of the role of long-range hydrodynamics,” *Physical Review Fluids* **3**, 042301 (2018).
- Giesekus, H., “Elasto-viskose flüssigkeiten, für die in stationären schichtströmungen sämtliche normalspannungskomponenten verschieden groß sind,” *Rheologica Acta* **2**, 50–62 (1962).
- Goddard, J., “The stress field of slender particles oriented by a non-newtonian extensional flow,” *Journal of Fluid Mechanics* **78**, 177–206 (1976a).
- Goddard, J. D., “Tensile stress contribution of flow-oriented slender particles in non-newtonian fluids,” (1976b).
- Goto, S., Nagazono, H., and Kato, H., “The flow behavior of fiber suspensions in newtonian fluids and polymer solutions.” *Rheologica acta* **25**, 119–129 (1986).
- Hassanpour, M., Shafigh, P., and Mahmud, H. B., “Lightweight aggregate concrete fiber reinforcement—a review,” *Construction and Building Materials* **37**, 452–461 (2012).
- Hinch, E. and Leal, L., “Time-dependent shear flows of a suspension of particles with weak brownian rotations,” *Journal of Fluid Mechanics* **57**, 753–767 (1973).
- Hinch, E. and Leal, L., “Constitutive equations in suspension mechanics. part 1. general formulation,” *Journal of Fluid Mechanics* **71**, 481–495 (1975).
- Hinch, E. and Leal, L., “Constitutive equations in suspension mechanics. part 2. approximate forms for a suspension of rigid particles affected by brownian rotations,” *Journal of Fluid Mechanics* **76**, 187–208 (1976).
- Huang, W.-X., Shin, S. J., and Sung, H. J., “Simulation of flexible filaments in a uniform flow by the immersed boundary method,” *Journal of computational physics* **226**, 2206–2228 (2007).
- Jeffery, G. B., “The motion of ellipsoidal particles immersed in a viscous fluid,” *Proceedings of the Royal Society of London. Series A, Containing papers of a mathematical and physical character* **102**, 161–179 (1922).
- Keshtkar, M., Heuzey, M., and Carreau, P., “Rheological behavior of fiber-filled model suspensions: Effect of fiber flexibility,” *Journal of Rheology* **53**, 631–650 (2009).
- Khan, M., More, R. V., Banaei, A. A., Brandt, L., and Ardekani, A. M., “Rheology of concentrated suspension of fibers with load dependent friction coefficient,” (2021),

- arXiv:2106.07702 [physics.flu-dyn].
- Kitano, T. and Kataoka, T., “The rheology of suspensions of vinylon fibers in polymer liquids. i. suspensions in silicone oil,” *Rheologica Acta* **20**, 390–402 (1981).
- Leal, L. and Hinch, E., “The effect of weak brownian rotations on particles in shear flow,” *Journal of Fluid Mechanics* **46**, 685–703 (1971).
- Lindström, S. B. and Uesaka, T., “Simulation of the motion of flexible fibers in viscous fluid flow,” *Physics of fluids* **19**, 113307 (2007).
- Lindström, S. B. and Uesaka, T., “Simulation of semidilute suspensions of non-brownian fibers in shear flow,” *The Journal of chemical physics* **128**, 024901 (2008).
- Lobry, L., Lemaire, E., Blanc, F., Gallier, S., and Peters, F., “Shear thinning in non-brownian suspensions explained by variable friction between particles,” *Journal of Fluid Mechanics* **860**, 682–710 (2019).
- Lundell, F., Söderberg, L. D., and Alfredsson, P. H., “Fluid mechanics of papermaking,” *Annual Review of Fluid Mechanics* **43**, 195–217 (2011).
- Mari, R., Seto, R., Morris, J. F., and Denn, M. M., “Shear thickening, frictionless and frictional rheologies in non-brownian suspensions,” *Journal of Rheology* **58**, 1693–1724 (2014).
- More, R. and Ardekani, A., “A constitutive model for sheared dense suspensions of rough particles,” *Journal of Rheology* **64**, 1107–1120 (2020a).
- More, R. V. and Ardekani, A. M., “Effect of roughness on the rheology of concentrated non-brownian suspensions: A numerical study,” *Journal of Rheology* **64**, 67–80 (2020b).
- Peskin, C. S., “Flow patterns around heart valves: a numerical method,” *Journal of computational physics* **10**, 252–271 (1972).
- Petrich, M. P., Koch, D. L., and Cohen, C., “An experimental determination of the stress–microstructure relationship in semi-concentrated fiber suspensions,” *Journal of non-newtonian fluid mechanics* **95**, 101–133 (2000).
- Petrie, C. J., “The rheology of fibre suspensions,” *Journal of Non-Newtonian Fluid Mechanics* **87**, 369–402 (1999).
- Phan-Thien, N. and Graham, A., “A new constitutive model for fibre suspensions: flow past a sphere,” *Rheologica acta* **30**, 44–57 (1991).
- Phan-Thien, N., Zheng, R., and Graham, A., “The flow of a model suspension fluid past a sphere,” *Journal of statistical physics* **62**, 1173–1195 (1991).
- Pinelli, A., Omidyeganeh, M., Brücker, C., Revell, A., Sarkar, A., and Alinovi, E., “The pelskin

- project: part iv—control of bluff body wakes using hairy filaments,” *Meccanica* **52**, 1503–1514 (2017).
- Pipes, R. B., “Anisotropic viscosities of an oriented fiber composite with a power-law matrix,” *Journal of composite materials* **26**, 1536–1552 (1992).
- Pipes, R. B., Coffin, D. W., Shuler, S. F., and Šimáček, P., “Non-newtonian constitutive relationships for hyperconcentrated fiber suspensions,” *Journal of composite materials* **28**, 343–351 (1994).
- Pipes, R. B., Hearle, J., Beaussart, A., Sastry, A., and Okine, R., “A constitutive relation for the viscous flow of an oriented fiber assembly,” *Journal of composite materials* **25**, 1204–1217 (1991).
- Salahuddin, A., Wu, J., and Aidun, C., “Study of semidilute fibre suspension rheology with lattice-boltzmann method,” *Rheologica Acta* **52**, 891–902 (2013).
- Segel, L. A. and Handelman, G. H., *Mathematics applied to continuum mechanics* (SIAM, 2007).
- Sepehr, M., Carreau, P. J., Moan, M., and Ausias, G., “Rheological properties of short fiber model suspensions,” *Journal of Rheology* **48**, 1023–1048 (2004).
- Shaqfeh, E. S. and Fredrickson, G. H., “The hydrodynamic stress in a suspension of rods,” *Physics of Fluids A: Fluid Dynamics* **2**, 7–24 (1990).
- Silbert, L. E., “Jamming of frictional spheres and random loose packing,” *Soft Matter* **6**, 2918–2924 (2010).
- Singh, A., Mari, R., Denn, M. M., and Morris, J. F., “A constitutive model for simple shear of dense frictional suspensions,” *Journal of Rheology* **62**, 457–468 (2018).
- Snook, B., Davidson, L. M., Butler, J. E., Pouliquen, O., and Guazzelli, E., “Normal stress differences in suspensions of rigid fibres,” *Journal of fluid mechanics* **758**, 486 (2014).
- Stickel, J. J., Knutsen, J. S., Liberatore, M. W., Luu, W., Bousfield, D. W., Klingenberg, D. J., Scott, C. T., Root, T. W., Ehrhardt, M. R., and Monz, T. O., “Rheology measurements of a biomass slurry: an inter-laboratory study,” *Rheologica Acta* **48**, 1005–1015 (2009).
- Stover, C. A., Koch, D. L., and Cohen, C., “Observations of fibre orientation in simple shear flow of semi-dilute suspensions,” *Journal of Fluid Mechanics* **238**, 277–296 (1992).
- Sundararajakumar, R. and Koch, D. L., “Structure and properties of sheared fiber suspensions with mechanical contacts,” *Journal of Non-Newtonian Fluid Mechanics* **73**, 205–239 (1997).
- Switzer III, L. H. and Klingenberg, D. J., “Rheology of sheared flexible fiber suspensions via fiber-level simulations,” *Journal of Rheology* **47**, 759–778 (2003).

- Tapia, F., Shaikh, S., Butler, J. E., Pouliquen, O., and Guazzelli, E., “Rheology of concentrated suspensions of non-colloidal rigid fibres,” *Journal of Fluid Mechanics* **827** (2017).
- Wang, J., O’Gara, J. F., and Tucker III, C. L., “An objective model for slow orientation kinetics in concentrated fiber suspensions: Theory and rheological evidence,” *Journal of Rheology* **52**, 1179–1200 (2008).
- Williams, S. and Philipse, A., “Random packings of spheres and spherocylinders simulated by mechanical contraction,” *Physical Review E* **67**, 051301 (2003).
- Wu, J. and Aidun, C. K., “A numerical study of the effect of fibre stiffness on the rheology of sheared flexible fibre suspensions,” *Journal of fluid mechanics* **662**, 123–133 (2010).
- Wyart, M. and Cates, M. E., “Discontinuous shear thickening without inertia in dense non-brownian suspensions,” *Physical review letters* **112**, 098302 (2014).